Tetrahedron 76 (2020) 131549

Contents lists available at ScienceDirect

Tetrahedron

journal homepage: www.elsevier.com/locate/tet

Light and reduction responsive supra-amphiphile for controllable fluorescence based on Pillar[6]arene

Yitao Wu, Liqing Shangguan, Peiren Liu, Yuezhou Liu, Qi Li, Jiajun Cao, Huangtianzhi Zhu*

State Key Laboratory of Chemical Engineering, Center for Chemistry of High-Performance & Novel Materials, Department of Chemistry, Zhejiang University, Hangzhou, 310027, PR China

ARTICLE INFO

Article history:
Received 8 June 2020
Received in revised form
12 August 2020
Accepted 24 August 2020
Available online 27 August 2020

Keywords:
Supramolecular chemistry
Dual-stimuli responsiveness
Pillar[6]arenes
Host–guest recognition
Tetraphenyl ethylene

ABSTRACT

As increasing demands of smart fluorescent materials, developing new systems with controllable emissions is more essential. Here we report a pillar[6]arene and tetraphenylethene (TPE)-based supra-amphiphile, which shows dual-responsiveness and tunable emission intensity. By introducing azobenzene units to a TPE fluorophore, the fluorescence is quenched via photo-induced electron transfer, whereas the emission regains upon the complexation with pillar[6]arene. Benefited from the light and reduction responsiveness of azobenzene, the fluorescent intensity of the supra-amphiphile can be easily controlled. The self-assembly morphologies including nanoparticles and nanoribbons are also found upon external stimuli. This work shows a new method to construct smart fluorescent materials.

1. Introduction

Smart fluorescent materials have attracted many researchers in recent years [1], and these materials have lots of applications such as sensing [2], cell imaging [3] and light-harvesting [4]. Among the mechanisms of these smart fluorescent materials, aggregation-induced emission (AIE) is one of the most promising candidate due to its high quantum yield, controllability and simple preparation [5]. Tetraphenylethene (TPE) is an archetypal luminogen with a simple molecule structure but shows a splendid AIE effect. TPE has been widely investigated and exhibited superior AIE luminescent and mesomorphic properties [6]. Therefore, developing TPE-containing materials is more favorable for intriguing properties and practical applications.

Compared with covalently bonded materials, supra-amphiphiles, which are constructed by non-covalent interactions such as hydrogen bonds, π-π stacking, electrostatic interactions and hydrophobic interactions, provide more flexible approaches to prepare smart fluorescent materials [7–10]. Furthermore, most of the supra-amphiphiles are easily constructed and have reversible stimuli-responsiveness. Therefore, stimuli-responsive supra-amphiphiles have been widely studied and showed applications in various fields, including drug delivery, sensors and photophysical materials [11]. In these works, many external stimuli have been used in controlling supra-amphiphiles such as light [12], pH [13], redox [14] and heat [15]. Among these stimuli, light is the most attractive one due to its clean, efficient and controllable features [16]. Apart from light, the redox-responsiveness is also attractive, which can be applied in many fields like sensing [17] and cell imaging [18]. The combination of these two stimuli in supra-amphiphile is rarely reported [19]. Therefore, constructing a dual-responsive supra-amphiphile may provide a new system for smart luminescent materials.

Pillararenes and their derivatives [20] are a new class of macrocyclic hosts after crown ethers [21], cyclodextrins [22], calixarenes [23] and cucurbiturils [24]. Their repeating aromatic units connected by methylene bridges at the para-positions form unique symmetric pillar-shaped architectures with electron-rich cavities [25] The unique structures and easy functionalization of pillararenes have endowed them with various applications including adsorption, separation, sensing and transmembrane transportation [26]. Due to the wide applications and unique properties, combining pillararenes and TPE is a reliable method for fabricating smart fluorescent materials [27]. Herein, we used a water-soluble pillar[6]arene (**WP6**) and its host–guest recognition to construct a dual-responsive fluorescent material incorporated with a TPE and

* Corresponding author.
E-mail address: htzzhu@zju.edu.cn (H. Zhu).

https://doi.org/10.1016/j.tet.2020.131549
0040-4020/

azobenzene-containing fluorophore (**G**). Due to the photo-induced electron transfer (PET) effect from TPE to azobenzene moieties [28], **G** showed negligible fluorescence, and yet the emission was controllable by host–guest recognition [29], light irradiation and redox additives [30]. Combining the multiple controlling approaches and fast response, we believe this supra-amphiphile is a novel and reliable candidate for smart fluorescent materials.

2. Result and discussion

2.1. Synthesis of compound *G*

Under protection of argon, compound 6 (135 mg, 76.0 μmol) and trimethylamine (3.00 mL, 33.5 mmol) were refluxed in 50.0 mL of THF overnight. After cooling to room temperature, the precipitate was collected and washed with CH_2Cl_2 to obtain compound **G** (150 mg, yield 98.0%) as an orange solid, which showed low solubility in normal solvents. Mp: 276.5°C–277.2 °C. ^{1}H NMR (600 MHz, DMSO-d_6, 298 K) δ (ppm): 7.89 (d, J = 12 Hz, 16H), 7.73 (d, J = 6 Hz, 8H), 7.11 (br, 8H), 6.82 (br, 8H), 6.68 (br, 8H), 4.65 (s, 8H), 4.12 (br, 8H), 3.94 (br, 8H), 3.07 (s, 36H), 1.83 (m, 16H). ^{13}C NMR (101 MHz, DMSO-d_6, 298 K) δ (ppm): 162.0, 156.3, 152.8, 146.1, 136.6, 134.1, 132.0, 130.7, 125.0, 122.5, 115.3, 114.0, 67.5, 63.7, 51.9, 31.6. HRMS: m/z calcd for $[M - 4Br]^{4+}$ $C_{106}H_{124}O_8N_{12}^{4+}$, 423.4878, found 423.4901, error 2.3 ppm.

2.2. Studies of photoisomerization and the host-guest complex

Firstly, we explored the photoisomerization process of **G** by ^{1}H NMR spectroscopy (Fig. 1b). The signals related to the protons i and h of *trans*-azobenzene moiety around 8.40 ppm disappeared and the signals related to *cis*-azobenzene moiety around 7.50–7.70 ppm appeared. UV light experiments provided direct evidence for the photoisomerization transformation process (Fig. S23) and ^{1}H NMR spectra revealed that the ratio of *cis*-**G**:*trans*-**G** after irradiation of UV light for 30 min was about 8:1 (Fig. S22). These phenomena indicated that the photo-induced isomerization of **G** happened upon irradiation, which was consistent with previous reports [31].

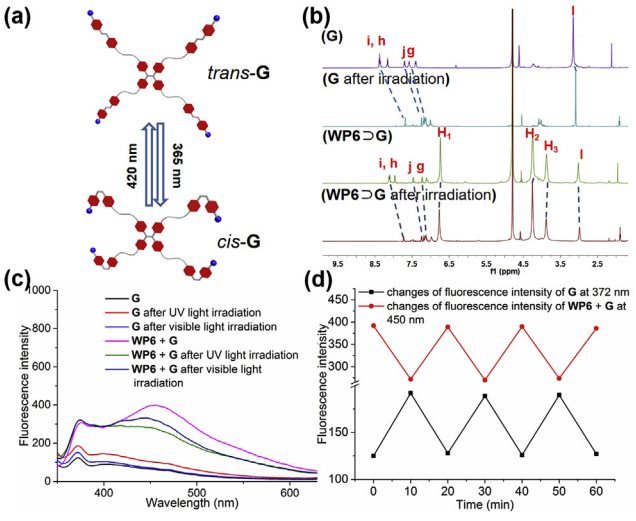

Fig. 1. (a) Cartoon representations of reversible photo-induced isomerization of *trans*-**G** and *cis*-**G**. (b) Partial ^{1}H NMR spectra (400 MHz, D_2O, 298 K) of **G** (3.00 mM) or **WP6⊃G** (3.00 mM) before and after irradiation in presence of 10% of DMSO-d_6. (c) Fluorescence spectra of **G** (1.00 mM in water) and **WP6⊃G** (1.00 mM in water) upon alternating irradiation with UV and visible lights. (d) Cyclic changes of the fluorescence intensity of **G** at 372 nm and **WP6⊃G** at 450 nm in fluorescence spectra upon alternating irradiation with UV and visible lights.

After studying the photoisomerization process of **G**, a dual-responsive supra-amphiphile based on the host–guest interactions between **WP6** and **G** was constructed. When **WP6** was added into an aqueous solution of **G**, the peaks in aryl region related to the azobenzene parts of **G** shifted upfield (Fig. 1b), indicating the host–guest complexation. The photo-responsiveness of **WP6⊃G** was also investigated, and the peaks corresponding to the guest (Fig. 1b, **WP6⊃G** after irradiation) displayed no obvious changes compared to the peaks related to free *cis*-***G*** (Fig. 1b, **G** after irradiation), indicating that the host-guest complex disassociated.

2.3. Fluorescence controlling via host-guest chemistry

After the establishment of **WP6⊃G** recognition motif, we further explored whether the host–guest recognition was able to control the fluorescence. According to the fluorescence spectra (Fig. 1c), the fluorescence intensity of **G** was weak due to intramolecular PET effect from TPE to azobenzene moieties. However, the emission of **G** slightly increased after the irradiation of UV light. These results also demonstrated that **G** was responsive to light because of weakened electron-withdraw ability of the *cis*-azobenzene moiety [32]. Nevertheless, after adding **WP6** to a solution of **G**, a remarkable enhancement of the fluorescence intensity occurred (Fig. 1c). This could be explained that the PET effect from TPE core to azobenzene units was inhibited after the azobenzene units threaded into the electron-rich cavity of **WP6**. Moreover, the fluorescence intensity of **WP6⊃G** decreased after the irradiation of UV light and nearly regained to the previous level after further irradiation with visible light. This phenomenon was certainly contributed by the destroy of the host–guest complex under UV irradiation due to the formation of *cis*-azobenzene with bulk steric hindrance [33]. The de-threaded guest led the appearance of PET that caused fluorescence quenching [34]. Further irradiating with visible light benefited the reformation of *trans*-azobenzene and the fluorescent host–guest complex. The photoisomerization process of **WP6⊃G** could be repeated several times, endowing the smart host–guest system with light controllability (Fig. 1d).

2.4. The reduction of the model guest and complex

Apart from light-responsiveness, the reduction of azobenzene is also a promising way to control the fluorescence. It's known that azobenzene groups can be reduced and even cleaved in presence of reductive agents [35]. Therefore, a reduction procedure was applied for the supra-amphiphile. **G1** (the synthetic procedures of this model guest are shown in supplementary materials) was designed as a model guest to firstly study the complicate reduction reaction. According to Fig. 2, upon the addition of $SnCl_2$, the peaks related to the protons e, d, f, c on **G1** disappeared and the peaks between 6.50 ppm and 7.80 ppm appeared (Fig. 2b). The new peaks in upfield region indicating the azobenzene part of **G1** was reduced, induced by the cleavage of azo bond and the increase of electron density of the azobenzene part. Similar reduction process was carried out on **WP6⊃G1** and we found that most of the peaks corresponding to the azobenzene moieties in host–guest complex shifted upfield after reduction (Fig. 2c and d). These results implied the reduction agent was able to reduce not only the model guest but also the host–guest complex. Moreover, the products of the reduction reaction were analyzed by mass spectroscopy (Fig. S26 and S27), and the results were consistent with the reduced azobenzene moiety.

2.5. Reduction-controlled fluorescence of the host-guest complex

After we knew $SnCl_2$ was capable of reducing azobenzene

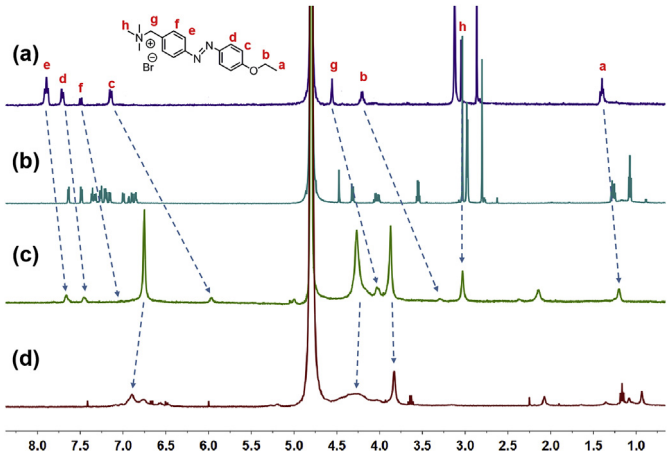

Fig. 2. ^{1}H NMR spectra (400 MHz, D_2O, 298 K) of **G1** (1.00 mM) before (a) and after (b) reduction. ^{1}H NMR spectra (400 MHz, D_2O, 298 K) of **WP6⊃G1** (1.00 mM) before (c) and after (d) reduction.

moiety, the reduction procedure was applied in reducing the supra-amphiphile. In Fig. 3b, a promoted emission was displayed by adding $SnCl_2$ to the aqueous solution of **G**. This phenomenon was ascribed to the reduction of the azobenzene moieties on **G**. Losing the azobenzene moiety weakened the PET process and at the same time promoted the aggregation of the hydrophobic TPE fluorophore, resulting in the increase of fluorescence. The similar fluorescence enhancement but yet lower intensity was found for the reduced **WP6** + **G** mixture. We assumed that the lower fluorescence intensity was attributed to the steric hindrance of **WP6**. Bulk **WP6** on the guest molecule decreased the reduction efficiency, which was also confirmed by time-dependent fluorescence intensity (Fig. 3c). Except for $SnCl_2$, similar experiments also had been carried out to confirm that **G** was responsive to different reductants (Fig. 3d). $SnCl_2$ exhibited the strongest redox ability among these reducing reagents, and the emission enhanced by azoreductase revealed that this system had potential in cell imaging, showing multiple ways to fulfill the redox-responsiveness.

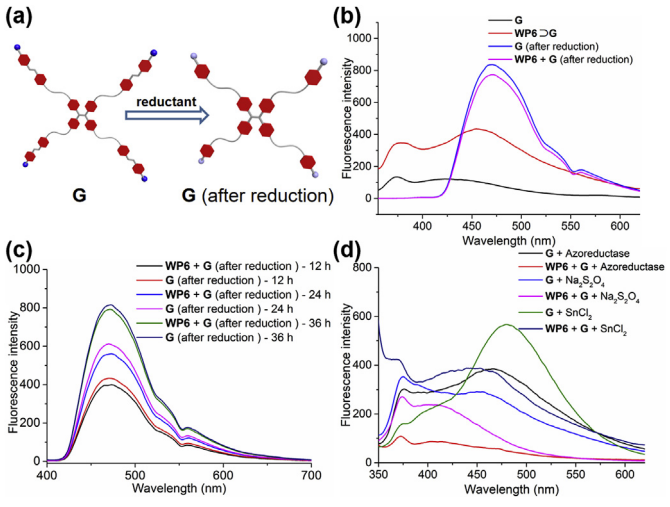

Fig. 3. (a) Cartoon representations of the reduction process of **G**. (b) Fluorescence spectra of **G** and **WP6⊃G** (0.05 mM) under the reduction condition. (c) Time-dependent fluorescence changes of **G** and **WP6⊃G** (0.05 mM) under the reduction condition. (d) Fluorescence spectra of **G** and **WP6⊃G** (0.05 mM) in present of different reducing agents.

2.6. Morphology studies

In addition, we explored the self-assembly behaviors of **G** and **WP6⊃G** in water. The self-assembly morphologies were observed by transmission electron microscopy (TEM), scanning electron microscopy (SEM) and atomic force microscopy (AFM). As shown in Fig. 4a and d, **G** self-assembled into nanoparticles with various sizes around 30 nm (Fig. S29), possibly driven by hydrophobic interactions. Even though **G** aggregated in water, weak fluorescence was observed due to PET effect as mentioned above. Adding **WP6** into the aqueous solution of **G** resulted in the formation of the supra-amphiphile **WP6⊃G**, which self-assembled into nanoparticles with an average diameter of 70 nm (Fig. S30). The image of SEM was in line with the TEM image (Fig. 4b and d). The formation of larger nanoparticles of supra-amphiphile could be explained by the changes of the amphiphilic building blocks, induced by bulk steric hindrance and electrostatic repulsion which were not able to form compact structures. Besides, the aggregated TPE cores emitted strong fluorescence after adding **WP6**, which was an evidence to the AIE effect. For the reduction responsiveness, adding $SnCl_2$ to **G** caused the morphology transformation from nanoparticles to nanoribbons with the thickness of 78.8 nm−106.6 nm (Fig. 4c and f and Fig. S31). A possible reason was that the amphiphilic reductive product of **G** formed multilayered nanoribbons in water driven by hydrophobic interaction and π−π interaction. When $SnCl_2$ was added to the solution of **G**, the lay-by-layer stacking of TPE cores established. Therefore, the nanoparticles changed into multilayered nanoribbons driven by hydrophobic interaction and the π−π interaction between the TPE cores and the hydrophilic ammonium terminated chain headed to water. UV spectroscopy provided evidence for this hypothesis (Fig. S36). The reductive product of **G** showed adsorption band between 300 and 365 nm corresponding to π−π* transition. The increase in intensity and red shifts in UV spectra were ascribed in part to the hypochromic effect due to interchain π−π stacking in an H-type aggregation form [36]. However, when the similar reductive procedure was applied for **WP6⊃G**, random aggregates were found on TEM (Fig. S26). The reduction of **WP6⊃G** produced large assemblies due to the partial de-threaded behavior or even the loss of azobenzene moiety.

3. Conclusion

In summary, we prepared a fluorescent supra-amphiphile with dual responsiveness and controllable emission intensity. The

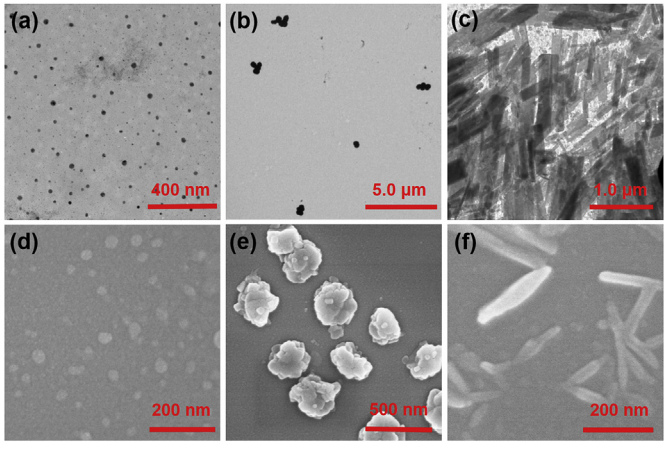

Fig. 4. TEM images of (a) **G**, (b) **WP6⊃G** and (c) **G** (after reduction) in water at 0.05 mM. SEM images of (d) **G**, (e) **WP6⊃G** and (f) **G** (after reduction) in water at 0.05 mM.

azobenzene-containing TPE fluorophore was synthesized, which showed weak emission due to the PET effect. Upon adding **WP6**, the formation of host–guest complexes inhibited the PET effect, rendering the supra-amphiphile with enhanced fluorescence. Moreover, the fluorescent intensity was easily modulated by light, resulting from the photoisomerization of azobenzene moieties. Apart from the photo-responsiveness, the reduction of azobenzene was also capable of controlling the fluorescence. We found that the supra-amphiphile exhibited increased fluorescence in presence of different reductants. Besides, the morphologies of **G** and the host–guest complex were also studied, which revealed the self-assemblies of nanoparticles and nanoribbons. This work shows a controllable fluorescent supra-amphiphile, and we believe it has potentials in smart fluorescent materials and devices.

4. Experimental section

4.1. Materials

Materials. All reagents were purchased and used directly. **WP6** was synthesized by following previously reported procedures [37].

4.2. Characterizations

UV–Vis adsorption spectroscopy UV–Vis sample of **G** (0.1 mM in deionized water) was prepared by irradiating with 365 nm UV light and analyzed on a Shimadzu UV-2550 instrument at room temperature.

Fluorescence emission spectroscopy. Samples of **G** (1.00 mM in water) and **WP6**⊃**G** (1.00 mM in water) for fluorescence spectra of photo-responsiveness were prepared by irradiating with 365 UV light or 435 visible light for 30 min. Samples of **G** (0.05 mM in water) and **WP6**⊃**G** (0.05 mM in water) for fluorescence spectra of reduction-responsiveness were prepared by adding 20.0 equivalent reductive agents into the original solution and stirred for 36 h and conducted on a RF-5301 spectrofluorophotometer (Shimadzu Corporation, Japan).

Scanning electron microscopy (SEM). SEM investigations were carried out on a JEOL 6390LV instrument. The SEM samples were prepared by drop-coating a solution of **G** (0.05 mM), a solution of **WP6**⊃**G** (0.05 mM), a solution of **G** (after reduction) (0.05 mM), or a solution of **WP6** + **G** (after reduction) (0.05 mM) onto silica wafers.

Transmission electron microscopy (TEM). TEM investigations were carried out on a JEM-1200EX instrument. The TEM samples were prepared by drop-coating a solution of **G** (0.05 mM), a solution of **WP6**⊃**G** (0.05 mM), a solution of **G** (after reduction) (0.05 mM), or a solution of **WP6** + **G** (after reduction) (0.05 mM) onto carbon-coated copper grids.

Atomic force microscopy (AFM). AFM samples were prepared by drop-coating a solution of **G** (0.05 mM), a solution of **WP6**⊃**G** (0.05 mM), or a solution of **G** (after reduction) (0.05 mM) onto silica wafers. AFM investigations were carried out on a Bruker Multimode 8 (see Scheme 1).

4.3. Synthetic procedures

The synthetic procedures are shown in Scheme 2 and discussed below.

4.3.1. Synthesis of compound 1

Compound **1** was prepared according to the previous report [38a]. 4-Aminobenzyl alcohol (5.00 g, 40.6 mmol) and hydrochloric acid (8.40 mL) were mixed in 70.0 mL of H_2O and stirred at 0 °C. An aqueous solution (18.0 mL) of $NaNO_2$ (5.30 g, 76.8 mmol) was added dropwise. The mixture was stirred for another 30 min after addition. Then, an aqueous solution (60.0 mL) of phenol (4.00 g, 42.5 mmol) and K_2CO_3 (8.00 g, 58.0 mmol) was added. After 4 h, the reaction was quenched by 100 mL of diluted acetic acid. The precipitate was collected and re-dissolved in acetone. After filtering, the filtrate was evaporated under vacuum to obtain the crude product, which was washed with methanol to get pure 1 as an orange solid (10.0 g, yield 64.8%). ^{1}H NMR (600 MHz, DMSO-d_6, 298 K) δ (ppm): 10.24 (s, 1H), 7.78 (d, J = 12 Hz, 4H), 7.47 (d, J = 12 Hz, 2H), 6.92 (d, J = 12 Hz, 2H), 5.31 (s, 1H), 4.56 (s, 2H).

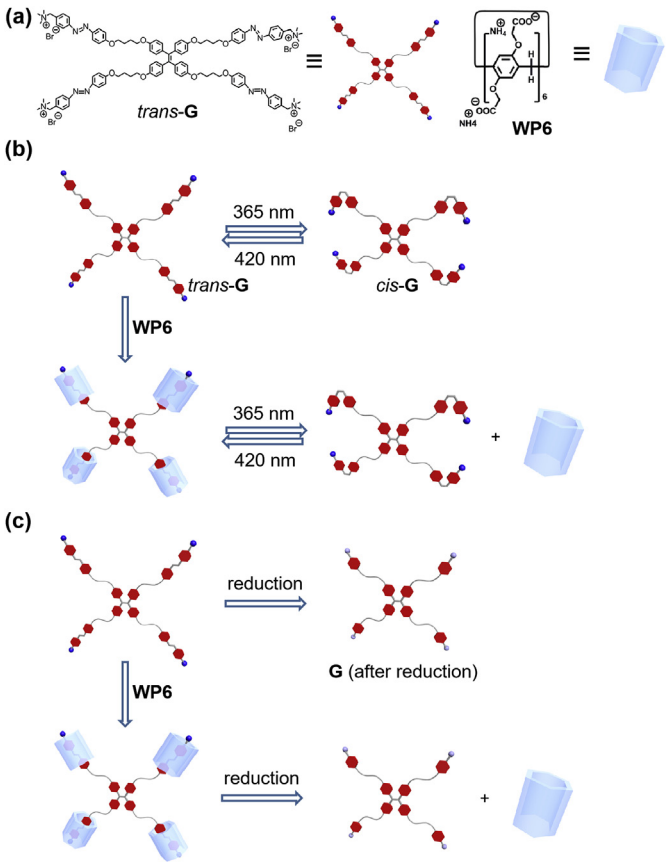

Scheme 1. (a) Chemical structures and cartoon representations of **G** and **WP6**. Cartoon representations of (b) the photo-responsive process and (c) the redox-responsive process.

4.3.2. Synthesis of compound 2

Compound **2** was prepared according to the previous report [38b]. $TiCl_4$ (45.0 mL, 400 mmol) were added dropwise into a mixture of THF (300 mL) and zinc powder (26.0 g, 400 mmol) at −70 °C. Then a solution of 4,4'-dimethoxybenzophenone (9.72 g, 40.0 mmol) in THF (20.0 mL) was added dropwise and the resulting mixture was heated in N_2 atmosphere at 90 °C for 2 days. After cooling to room temperature the mixture was hydrolyzed by adding aqueous K_2CO_3 solution (200 mL, 10.0%). The organic layer was collected and the aqueous layer was extracted with CH_2Cl_2 (300 mL). The combined organic layers were dried over $MgSO_4$ and evaporated. After purifying of the crude product by flash chromatography on SiO_2 (hexanes/ethylacetate = 10:1, *v*/*v*), the obtained solid was recrystallized from CH_2Cl_2/hexanes to get 7.30 g (yield 80.5%) of a pale yellow crystalline solid. ^{1}H NMR (400 MHz, $CDCl_3$, 298 K) δ (ppm): 6.93 (d, *J* = 8 Hz, 8H), 6.64 (d, *J* = 8 Hz, 8H), 3.74 (s, 12H).

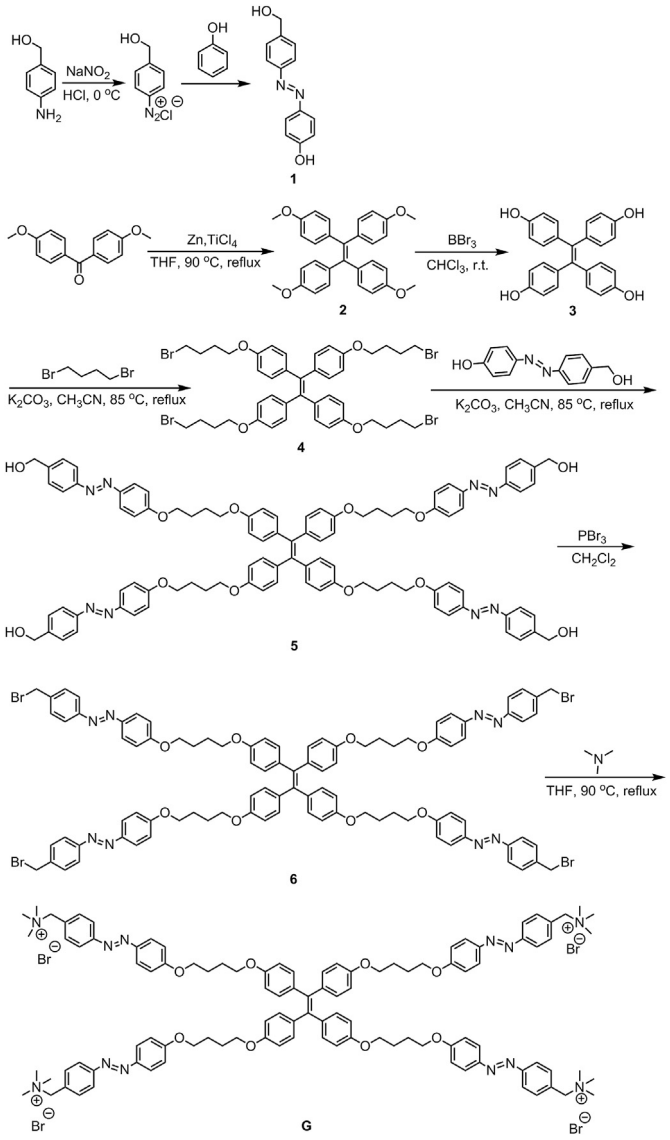

Scheme 2. Synthetic procedures of the TPE-bearing guest molecule.

*4.3.3. Synthesis of compound **3***

Compound **3** was prepared according to the previous report. [37b] BBr_3 (3.80 mL, 40.0 mmol) was added to a cooled solution of compound **2** (4.53 g, 10.0 mmol) in $CHCl_3$ (200 mL) at 0 °C and the resulting deep red mixture was stirred for 2 h at. After removal of the cooling bath, the mixture was stirred for 10 h at room temperature and then quenched by water. The precipitate was filtered, washed with H_2O and CH_2Cl_2. Recrystallization from EtOH/H_2O (1:1) obtained 3.29 g (yield 82.3%) of a light pink solid. ^{1}H NMR (400 MHz, DMSO-d_6, 298 K) δ (ppm): 9.22 (s, 4H), 6.70 (d, J = 8 Hz, 8H), 6.47 (d, J = 12 Hz, 8H).

*4.3.4. Synthesis of compound **4***

Compound **4** was prepared according to the previous report [38c]. Under the protection of argon, 1,4-dibromobutane (23.9 mL, 200 mmol) and K_2CO_3 (22.1 g, 160 mmol) were mixed and refluxed in 500 mL of CH_3CN in a three-neck flask. Compound **3** (3.96 g, 10.0 mmol) in 100 mL of CH_3CN was injected slowly. After 2 days, the mixture was filtered and the filtrate was concentrated under vacuum. The residue was purified by column chromatography using petroleum ether:ethyl acetate = 30:1 to 20:1 as eluent to obtain compound **4** as a white solid powder (6.02 g, yield 64.3%). ^{1}H NMR (600 MHz, $CDCl_3$, 298 K) δ (ppm): 6.91 (d, J = 6 Hz, 8H), 6.61 (d, J = 6 Hz, 8H), 3.92 (t, J = 6 Hz, 8H), 3.47 (t, J = 6 Hz, 8H), 2.05 (m, 8H), 1.90 (m, 8H).

*4.3.5. Synthesis of compound **5***

Under the protection of argon, compound **1** (3.29 g, 14.4 mmol) and K_2CO_3 (7.95 g, 57.6 mmol) were mixed in 500 mL of CH_3CN in a three-neck flask. The mixture was stirred and refluxed in the three-neck flask. Then, compound **4** (1.69 g, 1.80 mmol) in 100 mL CH_3CN was injected slowly. After 2 days, the mixture was filtered and the filtrate was concentrated under vacuum. The residue was purified by column chromatography using CH_2Cl_2:methanol = 20:1 as eluent to obtain compound **5** as an orange solid powder (420 mg, yield 15.3%). ^{1}H NMR (600 MHz, DMSO-d_6, 298 K) δ (ppm): 7.84 (d, J = 6 Hz, 8H), 7.78 (d, J = 6 Hz, 8H), 7.47 (d, J = 6 Hz, 8H), 7.07 (d, J = 12 Hz, 8H), 6.81 (d, J = 6 Hz, 8H), 6.67 (d, J = 6 Hz, 8H), 5.33 (s, 4H), 4.56 (s, 8H), 4.08 (t, J = 12 Hz, 8H), 3.93 (t, J = 12 Hz, 8H), 1.83 (m, 16H). ^{13}C NMR (151 MHz, DMSO-d_6, 298 K) δ (ppm): 164.4, 160.0, 154.1, 149.3, 148.6, 139.3, 135.2, 135.1, 135.0, 130.2, 127.5, 125.2, 118.1, 116.9, 70.9, 70.0, 65.9, 42.5, 32.6, 28.4. HRMS: m/z calcd for $[M + 2K + 2H]^{4+}$, $C_{94}H_{94}N_8O_{12}K_2^{4+}$, 401.0834, found 401.0832, error −1 ppm.

*4.3.6. Synthesis of compound **6***

To a solution of compound **5** (130 mg, 85.0 μmol) in 50.0 mL of dried CH_2Cl_2 was added PBr_3 (65.0 μL, 0.680 mmol) at −50 °C. The resulting mixture was stirred for 5 min at −50 °C and then 1 h at room temperature. After quenched by water, the organic layer was separated and concentrated to obtain **6** (135 mg, yield 89.4%) as an orange solid, which was used in the next step without further purification. ^{1}H NMR (600 MHz, $CDCl_3$, 298 K) δ (ppm): 7.89 (d, J = 6 Hz, 8H), 7.84 (d, J = 6 Hz, 8H), 7.51 (d, J = 6 Hz, 8H), 6.98 (d, J = 6 Hz, 8H), 6.93 (d, J = 6 Hz, 8H), 6.64 (d, J = 6 Hz, 8H), 4.54 (s, 8H), 4.10 (t, J = 6 Hz, 8H), 3.97 (t, J = 6 Hz, 8H), 1.81 (m, 16H). ^{13}C NMR (151 MHz, $CDCl_3$, 298 K) δ (ppm): 164.4, 155.2, 149.8, 142.8, 135.2, 132.5, 127.8, 125.7, 117.4, 116.2, 70.7, 70.0, 35.6, 125.6, 32.3, 28.6, 25.3, 16.6, 3.7, 2.6. MALDI-TOF MS: m/z calcd for $[M + H]^+$ $C_{94}H_{89}N_8O_8Br_4^+$, 1777.0185, found 1777.0160.

Declaration of competing interest

The authors declare that they have no competing financial interests or personal relationships that could have appeared to influence the work reported in this paper.

Acknowledgments

This work was supported by the Fundamental Research Funds for the Central Universities.

Appendix A. Supplementary data

Supplementary data to this article can be found online at https://doi.org/10.1016/j.tet.2020.131549.

Supplementary Material

^{1}H and ^{13}C NMR spectra, mass spectra, and other materials. Supplementary data related to this article can be found at http://xx.

References

[1] (a) C. Bao, L. Zhu, Q. Lin, H. Tian, Adv. Mater. 27 (2015) 1647–1662;

(b) Z. Yang, A. Sharma, J. Qi, X. Peng, D. Lee, R. Hu, D. Lin, J. Qu, J. Kim, Chem. Soc. Rev. 45 (2016) 4651–4667;
(c) Z. Yang, Z. Mao, Z. Xie, Y. Zhang, S. Liu, J. Zhao, J. Xu, Z. Chi, M. Aldred, Chem. Soc. Rev. 46 (2017) 915–1016.
[2] J.-P. Kim, Z. Xie, M. Creer, Z. Liu, J. Yang, Chem. Sci. 8 (2017) 550–558.
[3] N.-W. Pino, J. Davis, Z. Yu, J. Chan, J. Am. Chem. Soc. 139 (2017) 18476–18479.
[4] (a) I.-S. Park, S.-Y. Lee, C. Adachi, T. Yasuda, Adv. Funct. Mater. 26 (11) (2016) 1813–1821;
(b) K. Acharyya, S. Bhattacharyya, H. Sepehrpour, S. Chakraborty, S. Lu, B. Shi, X. Li, P.S. Mukherjee, P.J. Stang, J. Am. Chem. Soc. 141 (37) (2019) 14565–14569.
[5] R. Hu, N. Leung, B.-Z. Tang, Chem. Soc. Rev. 43 (2014) 4494–4562.
[6] X. Yan, P. Wei, Y. Liu, M. Wang, C. Chen, J. Zhao, G. Li, M.L. Saha, Z. Zhou, Z. An, X. Li, P.J. Stang, J. Am. Chem. Soc. 141 (24) (2019) 9673–9679.
[7] X. Zhang, C. Wang, Chem. Soc. Rev. 40 (2011) 94–101.
[8] Y. Chang, Y. Jiao, H.-E. Symons, J.-F. Xu, C.-F.-J. Faul, X. Zhang, Chem. Soc. Rev. 48 (2019) 989–1003.
[9] X.-M. Chen, Y. Chen, Q. Yu, B.-H. Gu, Y. Liu, Angew. Chem. Int. Ed. 57 (2018) 38, 12519–12523.
[10] G. Ouyang, M. Liu, Mater. Chem. Front. 4 (2020) 155–167.
[11] (a) K. Raghupathi, J. Guo, O. Munkhbat, P. Rangadurai, S. Thayumanavan, Acc. Chem. Res. 47 (2014) 4332–4353;
(b) H. Zhu, L. Shangguan, D. Xia, J. Modal, B. Shi, Nanoscale 9 (2017) 8913–8917.
[12] (a) L. Shao, B. Hua, J. Sun, Q. Li, J. Yang, G. Yu, Tetrahedron Lett. 58 (2017) 1863–1867;
(b) Z. Sun, G. Liu, J. Hu, S. Liu, Biomacromolecules 19 (2018) 2071–2081.
[13] (a) Z. Li, J. Yang, G. Yu, J. He, Z. Abliz, F. Huang, Chem. Commun. *50* (2014) 2841–2843;
(b) X. Wu, Y. Li, C. Lin, X.-Y. Hu, L. Wang, Chem. Commun. 51 (2015) 6832–6835.
[14] (a) D. Cao, M. Amelia, G. Klivansky, S.I. Koshkakaryan, M. Khan, S. Semeraro, M. Silvi, A. Venturi, A. Credi, Y. Liu, J. Am. Chem. Soc. 132 (3) (2010) 1110–1122;
(b) Y. Chang, K. Yang, P. Wei, W. Zhao, Z. Pei, Angew. Chem. Int. Ed. 53 (2014) 13126–13130.
[15] (a) B. Shi, D. Xia, Y. Yao, Chem. Commun. *50* (2014) 13932–13935;
(b) N. Song, D. Chen, Y. Qiu, X. Yang, B. Xu, W. Tian, Y.-W. Yang, Chem. Commun. 50 (2014) 8231–8234;
(c) J. Bi, X. Zeng, D. Tian, H. Li, Org. Lett. 18 (2016) 1092–1095.
[16] Y. Wang, Y. Zhang, Y. Liu, J. Am. Chem. Soc. 137 (2015) 4543–4549.
[17] W. Zang, C. Yang, T. Li, L. Liao, X. Zheng, Proc. Natl. Acad. Sci. Unit. States Am. 116 (51) (2019) 25624–25633.
[18] (a) Q. Cai, T. Yu, W. Zhu, Y. Xu, X. Qian, Chem. Commun. 51 (2015) 14739–14741;
(b) B. Shi, K. Jie, Y. Zhou, J. Zhou, D. Xia, F. Huang, J. Am. Chem. Soc. 138 (2016) 80–83.
[19] K. Wang, D.-S. Guo, X. Wang, Y. Liu, ACS Nano 5 (4) (2011) 2880–2894.
[20] (a) T. Ogoshi, S. Kanai, S. Fujinami, T. Yamagishi, Y. Nakamoto, J. Am. Chem. Soc. 130 (2008) 5022–5023;
(b) T. Ogoshi, T. Kakuta, T. Yamagishi, Angew. Chem. Int. Ed. 58 (8) (2019) 2197–2206;
(c) L. Chen, Y. Cai, W. Feng, L. Yuan, Chem. Commun. 55 (2019) 7883–7898;
(d) K. Du, A.C.-H. Sue, Synlett 30 (2019) 2209–2215.
[21] C.J. Pedersen, Angew. Chem., Int. Ed. Engl. 27 (1988) 1021–1027;
(b) H. Gibson, N. Yamguchi, J. Jones, J. Am. Chem. Soc. 125 (2003) 3522–3533.
[22] (a) G. Crini, Chem. Rev. 114 (2014) 10940–10975;
(b) Y. Wu, R. Shi, Y. Wu, J. Holcroft, Z. Liu, M. Frasconi, M. Wasielewski, H. Li, F. Stoddart, J. Am. Chem. Soc. 137 (2015) 4111–4118.
[23] D.-S. Guo, Y. Liu, Chem. Soc. Rev. 41 (2012) 5907–5921.
[24] K. Assaf, W. Nau, Chem. Soc. Rev. 44 (2015) 394–418.
[25] H. Zhang, Z. Liu, Y. Zhao, Chem. Soc. Rev. 47 (2018) 5491–5528.
[26] (a) D. Dai, Z. Li, J. Yang, C. Wang, J. Wu, Y. Wang, D. Zhang, Y.-W. Yang, J. Am. Chem. Soc. 141 (11) (2019) 4756–4763;
(b) D. Cao, Y. Kou, J. Liang, Z. Chen, L. Wang, H. Meier, Angew. Chem. Int. Ed. 48 (2009) 9721–9723.
[27] Q. Li, H. Zhu, F. Huang, J. Am. Chem. Soc. 141 (2019) 34, 13290–13294.
[28] K. Kiyose, K. Hanaoka, D. Oushiki, T. Nakamura, M. Kajimura, M. Sumatsu, H. Nishimatsu, T. Yamane, T. Terai, Y. Hirata, T. Nagano, J. Am. Chem. Soc. 132 (2010) 15846–15848.
[29] (a) L. Shao, B. Hua, J. Yang, G. Yu, Chem. Commun. 52 (2016) 6573–6576;
(b) C. Li, Q. Xu, J. Li, F. Yao, X. Jia, Org. Biomol. Chem. 8 (2010) 1568–1576.
[30] A. Samanta, B.J. Ravoo, Chem. Eur J. 20 (2014) 4966–4973.
[31] T. Xiao, L. Qi, W. Zhong, C. Lin, R. Wang, L. Wang, Mater. Chem. Front. 3 (2019) 1973–1993.
[32] H. Zhang, F. Liang, Y.-W. Yang, Chem. Eur J. *26* (2020) 198–205.
[33] G. Yu, C. Han, Z. Zhang, J. Chen, X. Yan, B. Zheng, S. Liu, F. Huang, J. Am. Chem. Soc. 134 (2012) 8711–8717.
[34] T.-J. Dale, J. Rebek, J. Jones, J. Am. Chem. Soc. 128 (14) (2003) 4500–4501.
[35] T. Sun, L. Shu, J. Shen, C. Ruan, Z. Zhao, C. Jiang, RSC Adv. *6* (2016) 52189–52200.
[36] (a) Z. Peng, K. Huang, Y. Tao, X. Li, L. Zhang, P. Lu, Y. Wang, Mater. Chem. Front. 1 (2017) 1858–1865;
(b) R. Maragani, R. Sharma, R. Misra, ChemistrySelect 2 (2017) 10033–10037.
[37] G. Yu, M. Xue, Z. Zhang, J. Li, C. Han, F. Huang, J. Am. Chem. Soc. 134 (2012) 13248–13251.
[38] (a) J. Kim, M. El-Khouly, Y. Araki, O. Ito, K. Kay, Chem. Lett. 37 (2008) 544–545;
(b) S. Andreas, D. Siegmar, L. Sabine, N. Manfred, Adv. Funct. Mater. 11 (6) (2001) (December);
(c) J. Li, K. Shi, D. Markus, B. Tang, J. Huang, Y. Yan, Chem. Commun. 52 (2016) 12466–12469.